

Provided for non-commercial research and education use.
Not for reproduction, distribution or commercial use.



This article appeared in a journal published by Elsevier. The attached copy is furnished to the author for internal non-commercial research and education use, including for instruction at the authors institution and sharing with colleagues.

Other uses, including reproduction and distribution, or selling or licensing copies, or posting to personal, institutional or third party websites are prohibited.

In most cases authors are permitted to post their version of the article (e.g. in Word or Tex form) to their personal website or institutional repository. Authors requiring further information regarding Elsevier's archiving and manuscript policies are encouraged to visit:

<http://www.elsevier.com/copyright>



Contents lists available at ScienceDirect

International Journal of Heat and Mass Transfer

journal homepage: www.elsevier.com/locate/ijhmt

Pool boiling heat transfer on the microheater surface with and without nanoparticles by pulse heating

Li Xu, Jinliang Xu*, Bin Wang, Wei Zhang

The Beijing Key Laboratory of New and Renewable Energy, North China Electric Power University, Beijing 102206, PR China

ARTICLE INFO

Article history:

Received 6 November 2010

Received in revised form 22 March 2011

Accepted 28 March 2011

Available online 29 April 2011

Keywords:

Nanofluids

Microheater

Bubble dynamics

Heat transfer

ABSTRACT

We study the pool boiling heat transfer on the microheater surface with and without nanoparticles by pulse heating. Nanofluids are the mixture of de-ionized water and Al_2O_3 particles with 0.1%, 0.2%, 0.5% and 1.0% weight concentrations. The microheater is a platinum surface by $50 \times 20 \mu\text{m}$. Three types of bubble dynamics were identified. The first type of bubble dynamics is for the boiling in pure water, referring to a sharp microheater temperature increase once a new pulse cycle begins, followed by a continuous temperature increase during the pulse duration stage. Large bubble is observed on the microheater surface and it does not disappear during the pulse off stage. The second type of bubble dynamics is for the nanofluids with 0.1% and 0.2% weight concentrations. The microheater surface temperature has a sharp increase at the start of a new pulse cycle, followed by a slight decrease during the pulse duration stage. Miniature bubble has oscillation movement along the microheater length direction, and it disappears during the pulse off stage. The third type of bubble dynamics occurs at the nanofluid weight concentration of 0.5% and 1.0%. The bubble behavior is similar to that in pure water, but the microheater temperatures are much lower than that in pure water. A structural disjoining pressure causes the smaller contact area between the dry vapor and the heater surface, decreasing the surface tension effect and resulting in the easy departure of miniature bubbles for the 0.1% and 0.2% nanofluid weight concentrations. For the 0.5% weight concentration of nanofluids, coalescence of nanoparticles to form larger particles is responsible for the large bubble formation on the heater surface. The microlayer evaporation heat transfer and the heat transfer mechanisms during the bubble departure process account for the higher heat transfer coefficients for the 0.1% and 0.2% nanofluid weight concentrations. The shortened dry area between the bubble and the heater surface, and the additional thin nanofluid liquid film evaporation heat transfer, account for the higher heat transfer coefficient for the 0.5% nanofluid weight concentration, compared with the pure water runs.

© 2011 Elsevier Ltd. All rights reserved.

1. Introduction

Nanofluid is envisioned to describe a fluid in which nanometer-sized particles are suspended in conventional heat transfer basic fluids [1]. The thermal conductivity of the particle materials, metallic or nonmetallic such as Al_2O_3 , CuO, SiO_2 , and TiO_2 , are typically order-of-magnitude higher than that of the base fluids even at low concentrations, resulting in significant increases in heat transfer coefficients. Single-phase liquid forced convection, as well as phase change heat transfer of nanofluids, have been widely studied [2,3].

Contradictory conclusions were reached on the boiling heat transfer of nanofluids in the literature. Bang and Chang [4] studied the boiling heat transfer of Al_2O_3 -water nanofluid on the copper plate with the planar size of $4 \times 100 \text{mm}^2$ and the thickness of

1.9 mm, and found that the effective nucleation site number is decreased due to the nanoparticles deposited on the copper surface, decreasing the nucleate heat transfer coefficients, but the critical heat flux (CHF) is increased. Golubovic et al. [5] investigated the boiling heat transfer of Al_2O_3 -water and BiO_2 -water nanofluid on the NiCr wire surface with the diameter of 0.64 mm and length of 50 mm. They found that the contact angle becomes smaller to enhance the critical heat flux due to the nanocoating effect on the wire surface. Kim et al. [6,7] systematically studied the effect of the porous layer on the wettability and contact angle, in which the porous layer is formed by the alumina, zirconia and silica nanoparticles on the heating surface. The critical heat flux is found to be raised, but the boiling heat transfer coefficients are not changed significantly. Dinh et al. [8] found the decreased bubble size, smaller wall temperatures, and more uniform wall temperature distribution, for the pool boiling heat transfer of Al_2O_3 - H_2O nanofluid than that for the pure liquid. Wen et al. [9,10] identified the significantly increased pool boiling heat transfer coefficients of Al_2O_3 -

* Corresponding author. Tel.: +86 10 61772268.

E-mail address: xjl@ncepu.edu.cn (J. Xu).

Nomenclature

A	heater area, m^2	V_1	voltages on the microheater, V
D_B	diameter of the dry zone, m	V_2	voltages in the precision resistance, V
D_b	bubble diameter, m	V_{film}	voltage on the platinum film, V
d	particle diameter, m	W	microheater width, m
F_g	buoyancy force, N	wt	weight concentration, %
F_i	inertia force, N	x	horizontal coordinate, m
$F_{\sigma 1}, F_{\sigma 2}$	surface tension force, N		
f	pulse frequency, Hz		
g	acceleration of gravity, m/s^2	<i>Greek symbols</i>	
h	liquid film thickness, m	δ	decay parameter
h_{lv}	latent heat of evaporation, kJ/kg	$\Delta\rho$	density difference between liquid and vapor, kg/m^3
I_{film}	electric current, A	θ	contact angle, $^\circ$
L	microheater length, m	κ	Debye length, m
nf	nanofluid	Π_0	amplitude coefficient of disjoining pressure, Pa
p	bulk osmotic pressure, Pa	Π_1	amplitude coefficient of disjoining pressure, Pa
p_l	pressure of the liquid, Pa	$\Pi(h)$	disjoining pressure of a film, Pa
p_v	pressure of the vapor gas, Pa	ρ_v	vapor density, kg/m^3
pw	pure water	σ	surface tension, N/m
Q_{film}	heating power on the heater film, W	τ	pulse duration time, ms
q_{film}	heat flux on the heater surface, MW/m^2	ϕ	volume concentration, %
R	precision resistance, Ω	ϕ_2	phase of oscillations, $^\circ$
R_{Au1}, R_{Au2}	gold film resistance, Ω	w	frequency of the oscillation, Hz
R_{film}	platinum film resistance, Ω		
T_{film}	heater surface temperature, $^\circ C$	<i>Subscripts</i>	
t	time, ms	l	liquid
		v	vapor

H_2O and TiO_2-H_2O nanofluids. Liu et al. [11] studied the pool boiling heat transfer of $CuO-H_2O$ nanofluid on the fin heat transfer surface under various pressure environments. The boiling heat transfer coefficients and critical heat fluxes are found to be increased by 25% and 50%, respectively, at the atmospheric pressure, but they are increased by 150% and 200%, respectively, under reduced pressure, for the nanofluids than those for the pure liquid. Kedzierskia and Gong [12] showed that the mixture of R134a liquid and CuO nanoparticles could significantly increase the heat transfer coefficient by 29.7%.

Several factors influence the boiling heat transfer in nanofluids. First, adding the dispersant liquid in the base fluid changes the physical properties of the base fluid. Besides, nanofluids with higher weight concentrations usually cause the particle coalescence and particle deposition on the heating surface. For the later cases, it is difficult to identify which mechanisms affect the boiling heat transfer, the nanofluids or the deposited particles on the heater surface.

In order to answer these questions, we use the nanofluids with weight concentrations of 0.1%, 0.2%, and 0.5% to perform the experiments. These concentrations cause no particle coalescence and deposition without dispersant liquid added. However, higher weight concentration of 1.0% was also used, which results in the particle deposition on the heater surface. A platinum microheater was used, which was driven by a pulse voltage generator. Three types of bubble dynamics were identified. The bubble dynamics is observed by a high speed camera bonded with a microscope. Physical explanations are given for the three types of bubble dynamics. It is well known that the periodic bubble behavior driven by pulse voltage generator has been widely used for various microfluidic actuators. The key issue for such kind of actuators is the high microheater temperatures during the heating stage. Mixing nanoparticles with pure liquid is helpful to maintain low microheater temperatures, preventing the microheater from dam-

age due to the high temperature. This study identifies that the nanofluids with uniformly distributed nanoparticles enhance the pool boiling heat transfer, corresponding to the low nanofluid concentrations such as smaller than 0.5%. However, high nanofluid weight concentration such as larger than 1.0% has poorer boiling heat transfer performance than the low weight concentrations, due to the deposited particles on the heater surface, but is still better than the pure water runs.

2. Description of the experiment

2.1. Preparation of nanofluids

The Al_2O_3 nanoparticles have spherical shape with the average diameter of 13 nm. These particles are dispersed in the de-ionized water by the ultrasonic oscillation method. Four weight concentrations of 0.1%, 0.2%, 0.5% and 1.0% are used, without dispersant fluid involved. The nanoparticles before the ultrasonic oscillation treatment are coalesced together to form the floc shape, as shown in Fig. 1a. On the contrary, the nanoparticles after the ultrasonic oscillation treatment is uniformly distributed for the weight concentrations of 0.1%, 0.2%, and 0.5%. Fig. 1b shows that no coalescence phenomenon is observed for the 0.2% weight concentration. However, for the weight concentrations of 1.0%, the particle coalescence is observed without the dispersant fluid involved (see Fig. 1c). In this study, because the nanoparticles have small size in the order of 10 nm, they are not settled down on the heater surface for the weight concentrations of 0.1%, 0.2%, and 0.5%. As observed in Fig. 1d, the heater surface is clean after several days of operation of experiments. However, nanoparticles indeed deposit on the heater surface and accumulate there after one day operation of experiments for the 1.0% weight concentration, as shown in Fig. 1e.

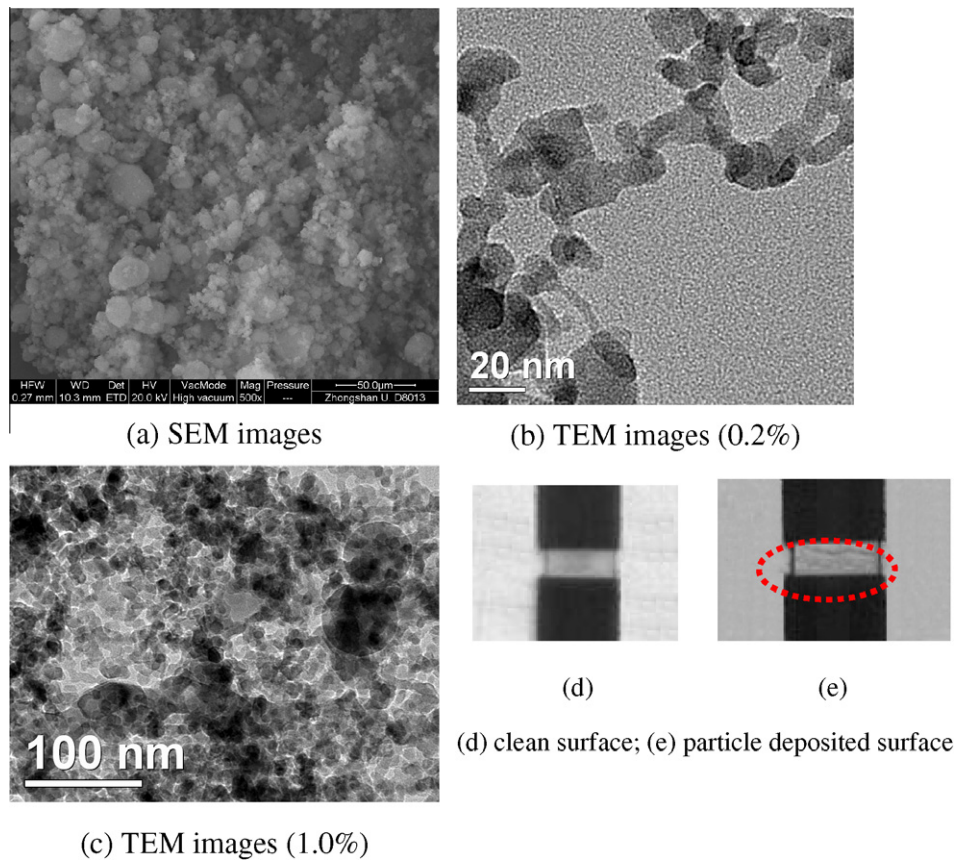


Fig. 1. SEM and TEM images of nanoparticles.

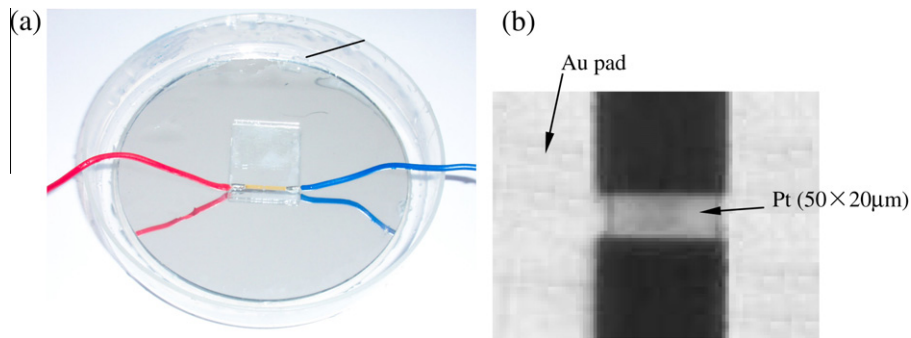


Fig. 2. The microheater immersed in glass beaker (a) and the microheater size (b).

2.2. The microheater and experimental setup

Fig. 2a shows the microheater test section. A glass beaker contains the nanofluid. The platinum microheater with the heating size of $50 \times 20 \mu\text{m}^2$ was fabricated on a 7740 Pyrex glass wafer. Fig. 2b shows the microheater size and the connected gold pad. The glass wafer was horizontally immersed in the nanofluid pool. The vertical distance between the glass wafer plane and the top fluid surface is about 1 cm.

The micro-fabrication technique is shortly described here. The photoresist was spun on a 7740 Pyrex glass wafer. After patterning with the technique of photolithography, a titanium layer of 200 Å, a platinum layer of 1500 Å and a gold layer of 3000 Å were sputtered successively on the wafer. After another process of photolithography, the technique of chemical etching was used to remove the gold to expose the platinum microheater, having the

length of 50 μm and width of 20 μm . Even though the heat flux on the microheater is high on the order of 100 MW/m², the heating power is small due to the small heating area. The pool nanofluid temperature remains constant during the experiment.

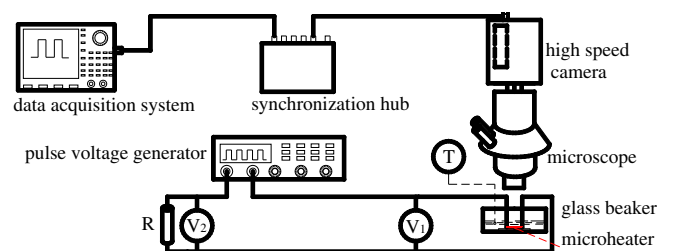


Fig. 3. The experimental setup.

Fig. 3 shows the experimental setup. The optical measurement system consists of a microscope bonded with a high speed camera, which detects the bubble dynamics. A pulse power generator drives the microheater for the pool boiling heat transfer. A high speed data acquisition system measures the voltage applied on the microheater and the electric resistance. A thermocouple measures the pool liquid temperature in the beaker. The optical measurement system and the high speed data acquisition system were synchronized by a synchronization hub, with the time resolution of 10 ns.

2.3. Data reduction and uncertainty analysis

Before the formal experiment, a calibration process was performed in an oven with precisely controlled temperature with the resolution of 1 °C. In order to ensure neglectable temperature rise of the microheater, the voltage applied on the microheater is on the magnitude of 10 mV, which is about two orders lower than that during the pool boiling experiment. The temperature and the microheater resistance have the following relationship as

$$T_{\text{film}} = 61.48R_{\text{film}} - 278.59 \quad (1)$$

During the experiment, by measuring the voltages V_1 on the microheater and V_2 on the precisely selective resistance, the platinum microheater resistance (not including the resistances of the two gold pads) is written as (see Fig. 2):

$$R_{\text{film}} = \frac{V_1}{V_2} R - R_{\text{Au1}} - R_{\text{Au2}} \quad (2)$$

where R_{Au1} and R_{Au2} are the two gold pad resistances, respectively (see Fig. 2). The current flowing through the microheater is

$$I_{\text{film}} = V_2 / R \quad (3)$$

where R is the precise resistance, equals to 5 Ω. The voltage and power on the microheater (not including the components on the two gold pads) are

$$V_{\text{film}} = V_1 - \frac{V_2}{R} (R_{\text{Au1}} + R_{\text{Au2}}) \quad (4)$$

$$Q_{\text{film}} = I_{\text{film}}^2 R_{\text{film}} = \left(\frac{V_2}{R}\right)^2 \left(\frac{V_1}{V_2} R - R_{\text{Au1}} - R_{\text{Au2}}\right) \quad (5)$$

The heat flux on the microheater is

$$q_{\text{film}} = Q_{\text{film}} / A = Q_{\text{film}} / (LW) \quad (6)$$

where L and W are the length and width of the microheater, respectively. Uncertainties of the voltage, heat flux and the resistance are 1 mV, 6.4% and 0.01%, respectively. The microheater temperature was estimated to have the uncertainty of 8.9 °C.

3. Experimental procedure

1. Determine the curve of the microheater resistance versus temperatures experimentally.
2. Inject de-ionized degassed water into the glass beaker, put the microheater test section under the water surface by 1 cm.
3. Fix the pulse frequency, pulse duration ratio (defined as the pulse duration time divided by the pulse cycle period), increase the voltage amplitude gradually.
4. Visualize the bubble dynamics near the microheater area. The voltage amplitude is fixed at which bubbles appeared on the microheater surface. The high speed data acquisition system, the optical system, and the pulse voltage generator are synchronized to work together to record the related data and image files.

5. Increase the voltage amplitude gradually. Repeat steps 3 and 4 to study the effect of the voltage amplitude on the bubble dynamics on the microheater surface.
6. Change the weight concentration of nanofluids at four values 0.1%, 0.2%, 0.5% and 1.0%. Repeat steps 3–5.

4. Results and discussion

4.1. The microheater temperatures

Fig. 4 shows the microheater temperatures versus time at different weight concentration of nanofluids. The pulse frequency is $f = 100$ Hz and the pulse duration time is $\tau = 0.75$ ms. The average heat flux on the microheater is $q_{\text{film}} = 93 \pm 80.5$ MW/m², neglecting the mini change of the heat flux during the heating stage. The microheater temperatures are significantly different for different weight concentration of nanofluids. For the pool boiling heat transfer in pure water, the temperatures are sharply increased to about 190 °C after a new pulse cycle begins. Then the temperatures are gradually increased to 250 °C at the end of the pulse duration time.

For the pool boiling of nanofluids with the weight concentration of 0.1%, the temperatures are sharply increased to about 160 °C, followed by a slight decrease of temperatures. The temperature oscillations with small amplitude are observed. The temperature response for the weight concentration of nanofluids of 0.2% is similar to that for the weight concentration of nanofluids of 0.1%, expect that the oscillation amplitude is quite larger for the nanofluid weight concentration of 0.2%.

When the weight concentrations of nanofluids are increased to 0.5% and 1.0%, the temperature curves are similar to that without nanoparticles. However, the temperatures are significantly lower for the nanofluid weight concentration of 0.5% than those with pure water, but are approaching the curve in pure water for the 1.0% weight concentration of nanofluids. The above temperature responses of the microheater correspond to the three types of bubble dynamics, which will be explained in the following subsections.

4.2. The first type of bubble dynamics for pool boiling of pure water

Fig. 5 shows the voltage, heat flux and temperatures of the microheater versus time in pure water without nanoparticles. Correspondingly, Fig. 6 shows the bubbles dynamics in a complete cycle. Because the microheater temperatures are increased during the whole pulse duration stage, the microheater resistance is

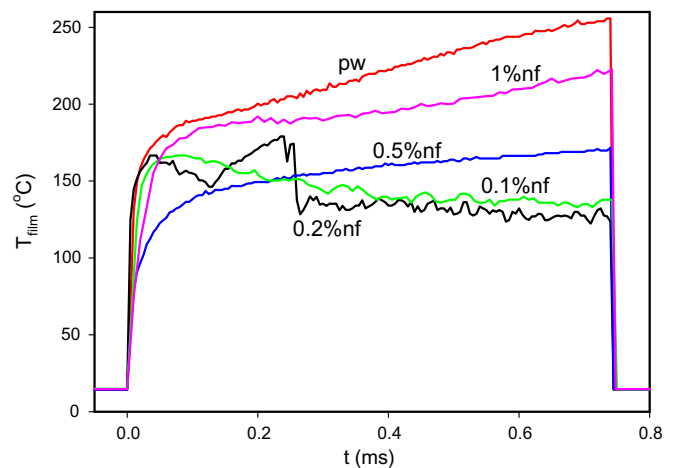


Fig. 4. Microheater temperature response at various nanofluid weight concentrations ($f = 100$ Hz, $\tau = 0.75$ ms, $q_{\text{film}} = 93 \pm 0.5$ MW/m²).

increased, resulting in a slight increase in the heat flux. Always there is a bubble on the microheater, during both the pulse duration stage and the pulse off stage in a full cycle. In other words, the bubble cannot be fully condensed when the pulse voltage is receded during the pulse off stage. Once a new pulse cycle starts, the initially existed bubble is further growing. The bubble nucleation

site is not needed, thus the “V” shape curve of the temperatures versus time reported in the literature [13,14] is not observed. It is observed that the “pre-existed bubble” on the microheater before a new pulse arrives is almost the same on the same condition. This is because the “pre-existed bubble” size is determined by the evaporation during the pulse on stage and condensation during the

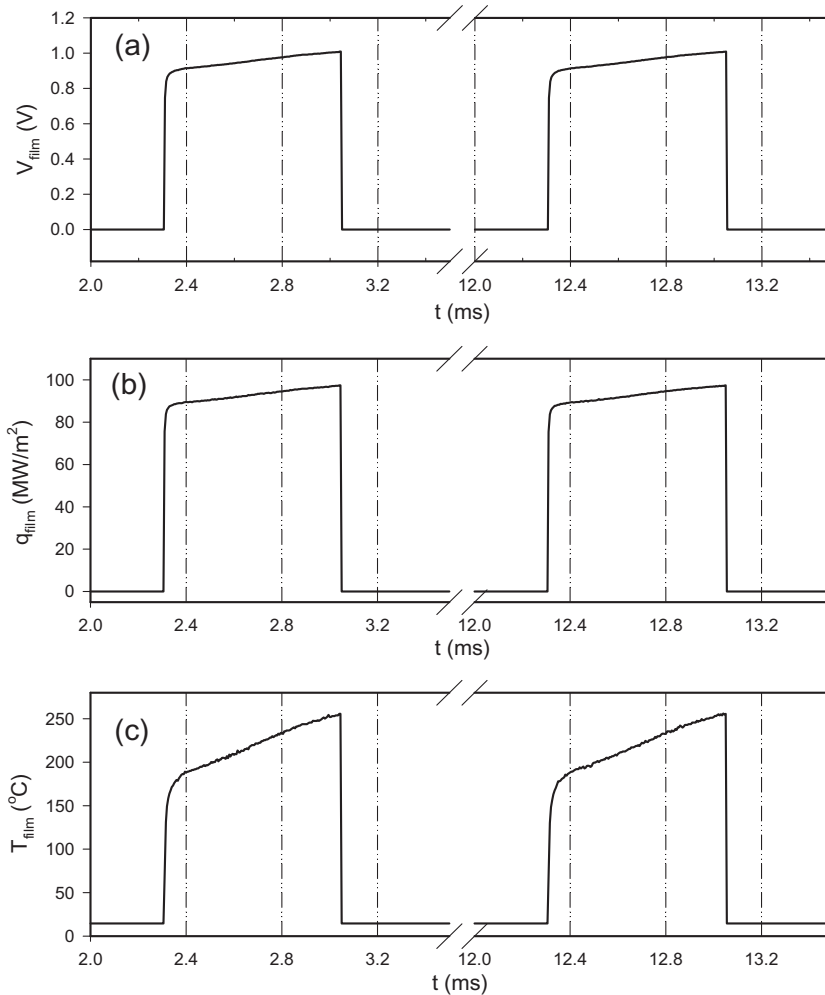


Fig. 5. Voltage, heat flux and temperature on the microheater surface in pure water ($f = 100$ Hz, $\tau = 0.75$ ms).

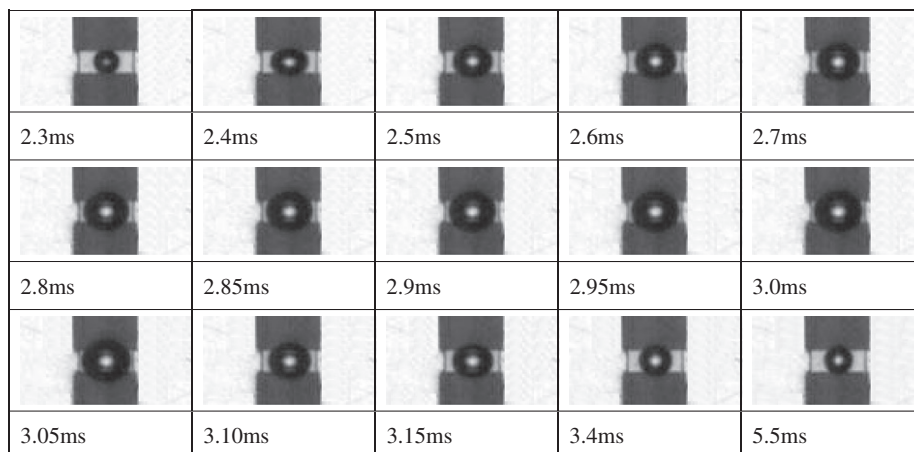


Fig. 6. Bubble dynamics in pure water for $f = 100$ Hz, $\tau = 0.75$ ms.

pulse off stage. But the “pre-existed bubble” is changed for different pulse heating parameters, quantified by the pulse cycle period, pulse duration time, and the voltage amplitude. This is the first type of bubble dynamics for the pool boiling heat transfer in pure water. Fig. 5 gives the parameters versus time for two successively cycles, showing the exactly repeated cyclic behavior.

4.3. The second type of bubble dynamics for pool boiling heat transfer of nanofluids

The microheater temperature response for the low weight concentration of 0.1% is given in Fig. 4 and is repeated in Fig. 7c for two successive cycles. The temperature is only slightly changed during the whole pulse duration stage, causing a small change of the microheater resistance. Thus the voltage and heat flux on the microheater are nearly not changed (see Fig. 7a and b). It is also observed that the bubble dynamics is roughly repeated for the two cycles. As shown in Fig. 8, the bubble dynamics is significantly different from that in pure water run shown in Fig. 6. The bubble dynamics displays the following characteristics: (1) The bubble disappears during the pulse off stage. (2) Much smaller bubble is observed during a whole pulse cycle. (3) The bubble has oscillation movement in the microheater length direction, against the microheater center.

As shown in Fig. 8, a tiny bubble appears at $t = 0.3$ ms but is moving toward the microheater center from left to right. The bubble is changing its movement direction frequently. It is growing up during the bubble oscillation movement. This is the second type of

bubble dynamics for the pool boiling heat transfer for low weight concentration of nanofluids.

A Small difference is identified for the pool boiling heat transfer between the weight concentrations of 0.1% and 0.2%. Figs. 9 and 10 illustrate the microheater temperatures and the bubble dynamics for the weight concentration of 0.2%. The temperature curves are roughly repeated with a small difference for two successive pulse cycles. As shown in Fig. 10, small bubbles are observed, similar to those found for the weight concentration of 0.1%. However, the vapor cloud caused by the vapor explosion is detected, such as shown at $t = 1.75$ ms in Fig. 10. The vapor cloud temporarily covers the area which is much larger than the microheater area.

4.4. The third type of bubble dynamics for pool boiling heat transfer of nanofluids

The third type of bubble dynamics for pool boiling heat transfer of nanofluids takes place for the weight concentrations of 0.5% and 1.0%. This type of bubble dynamics is similar to that of pure water without nanoparticles. Fig. 11 shows the voltage, heat flux, and temperatures of the microheater for the weight concentration of 0.5%. The temperatures are sharply increased to about 140 °C once a new pulse cycle starts, followed by a slight increase, until the maximum temperature of 170 °C is reached at the end of the pulse duration stage (see Fig. 11c). Even though the temperature curve for this type is similar to that of pure water, the temperatures are much lower than those of pure water without nanoparticles.

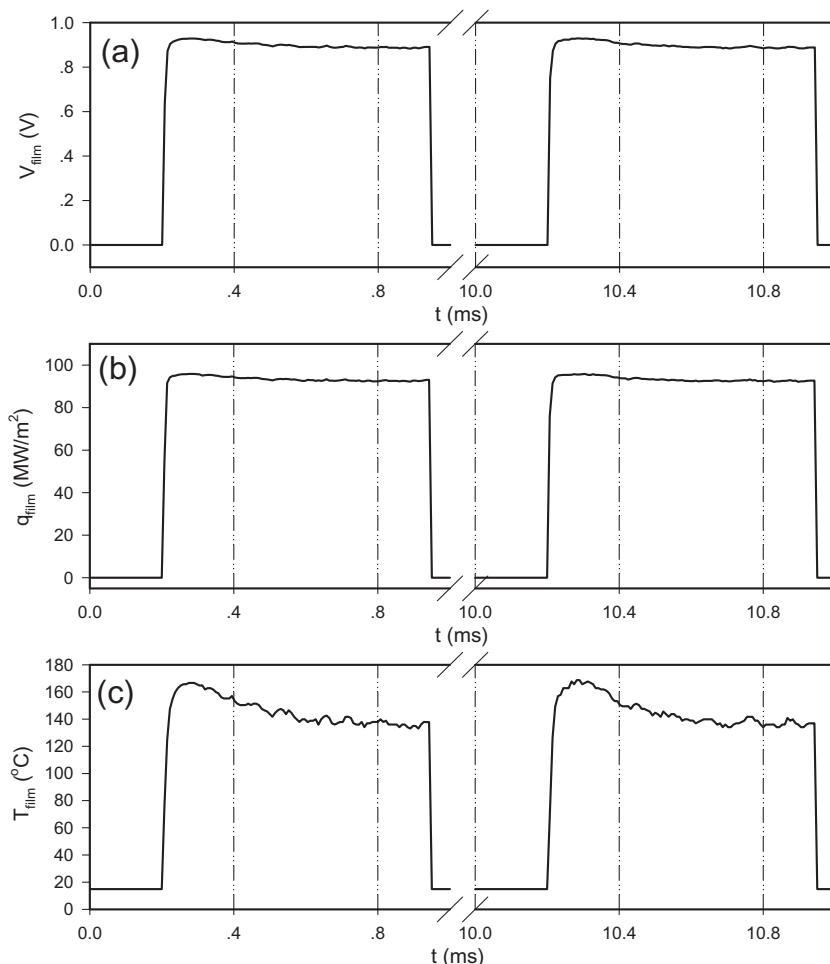


Fig. 7. Voltage, heat flux and temperature on the microheater surface with 0.1% nanofluid weight concentration ($f = 100$ Hz, $\tau = 0.75$ ms).

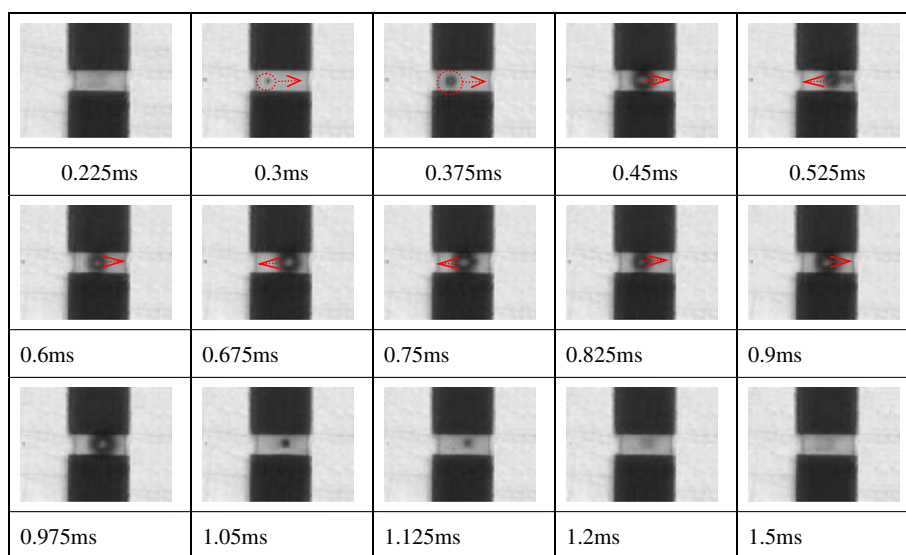


Fig. 8. Bubble images with 0.1% weight concentration of nanofluids ($f = 100$ Hz, $\tau = 0.75$ ms).

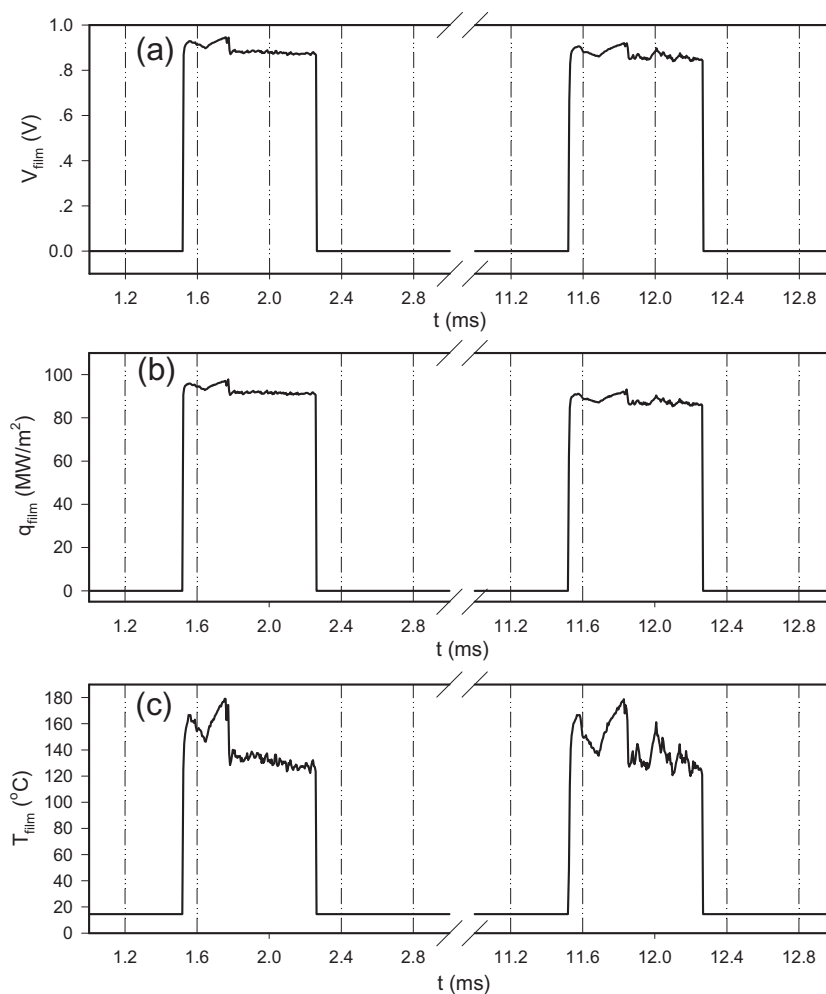


Fig. 9. Voltage, heat flux and temperature on the microheater surface with 0.2% nanofluid weight concentration ($f = 100$ Hz, $\tau = 0.75$ ms).

Due to the small change of the microheater temperatures, very slight changes of the voltage and heat flux versus time are observed during the whole pulse duration stage (see Fig. 11a and b). Fig. 12 shows the bubble images at different time. The bubble

on the microheater did not disappear during the pulse off stage, thus always there is a bubble on the microheater. The bubble is growing up once a new pulse cycle begins. The “pre-existed bubble” before a new pulse arrives has almost the same size for a

given set of pulse heating parameters (pulse frequency, pulse duration time, and voltage amplitude), but it is changed when the heating parameters are changed.

The above runs ($wt = 0\%$, 0.1% , 0.2% , and 0.5%) involve no particle deposition on the heater surface due to the low weight concentrations of nanofluids used. The microheater surface is clean after

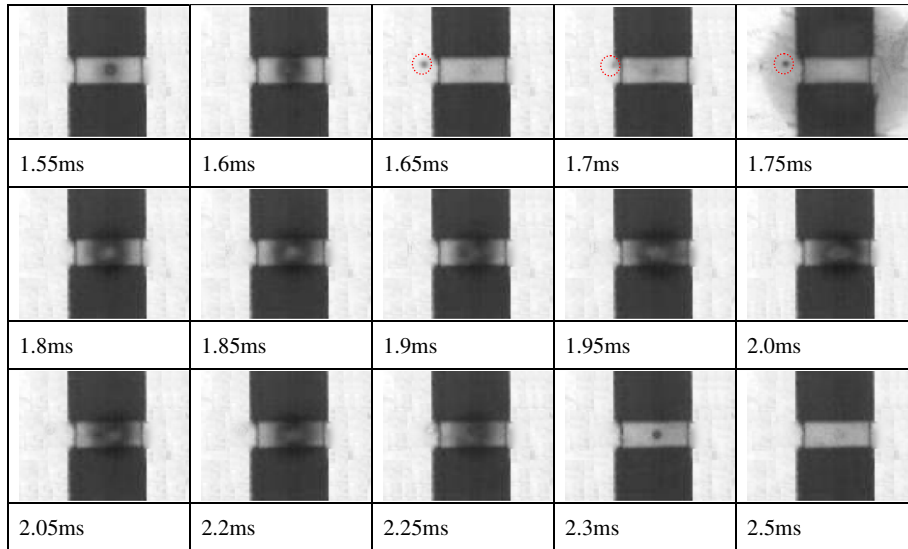


Fig. 10. Bubble images with 0.2% nanofluid weight concentration ($f = 100$ Hz, $\tau = 0.75$ ms).

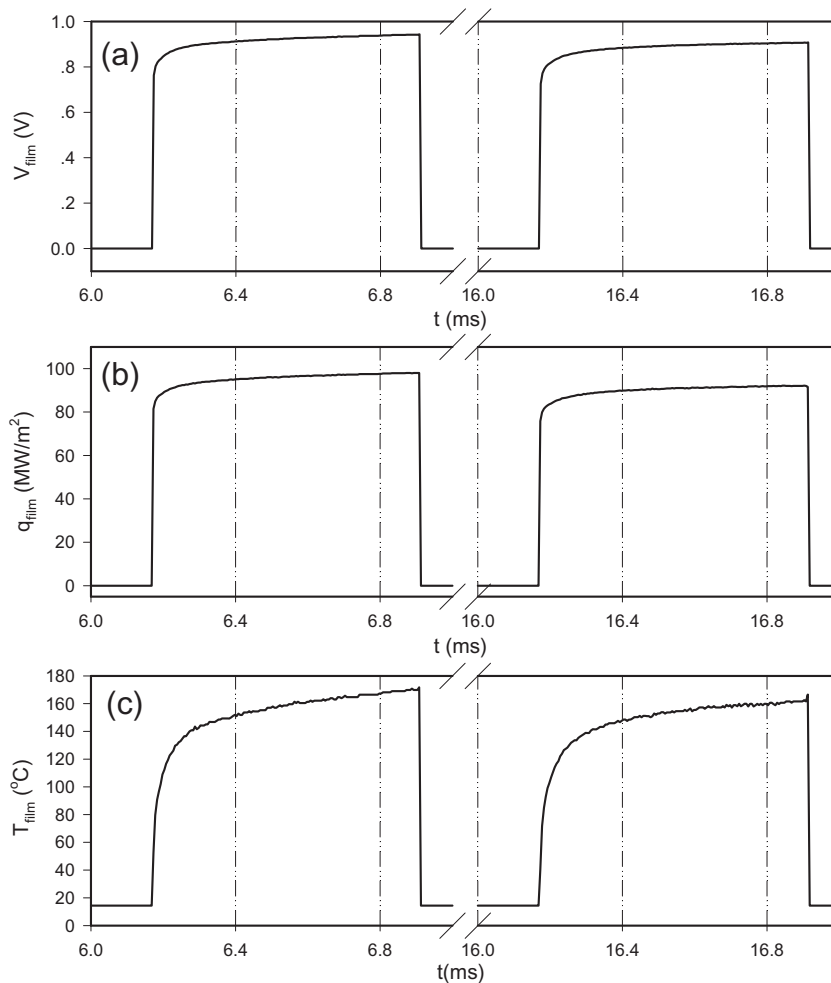


Fig. 11. Voltage, heat flux and temperature on the microheater surface with 0.5% nanofluid weight concentration ($f = 100$ Hz, $\tau = 0.75$ ms).

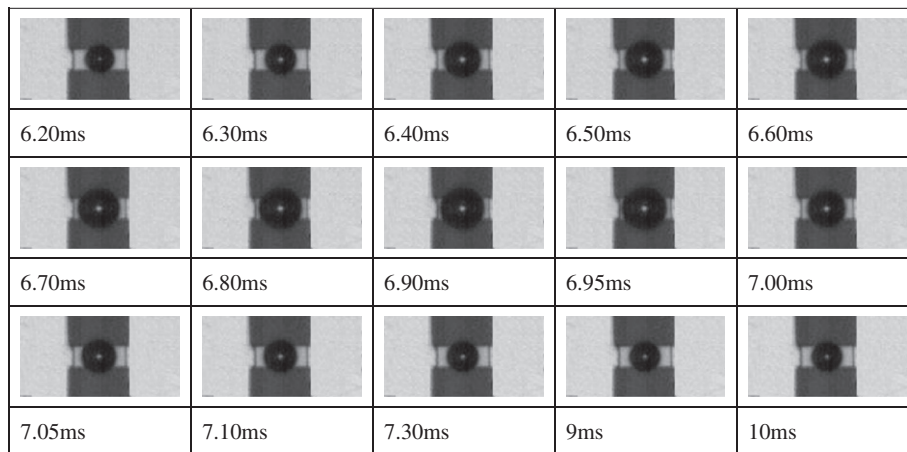


Fig. 12. Bubble images with 0.5% weight concentration of nanofluid ($f = 100$ Hz, $\tau = 0.75$ ms).

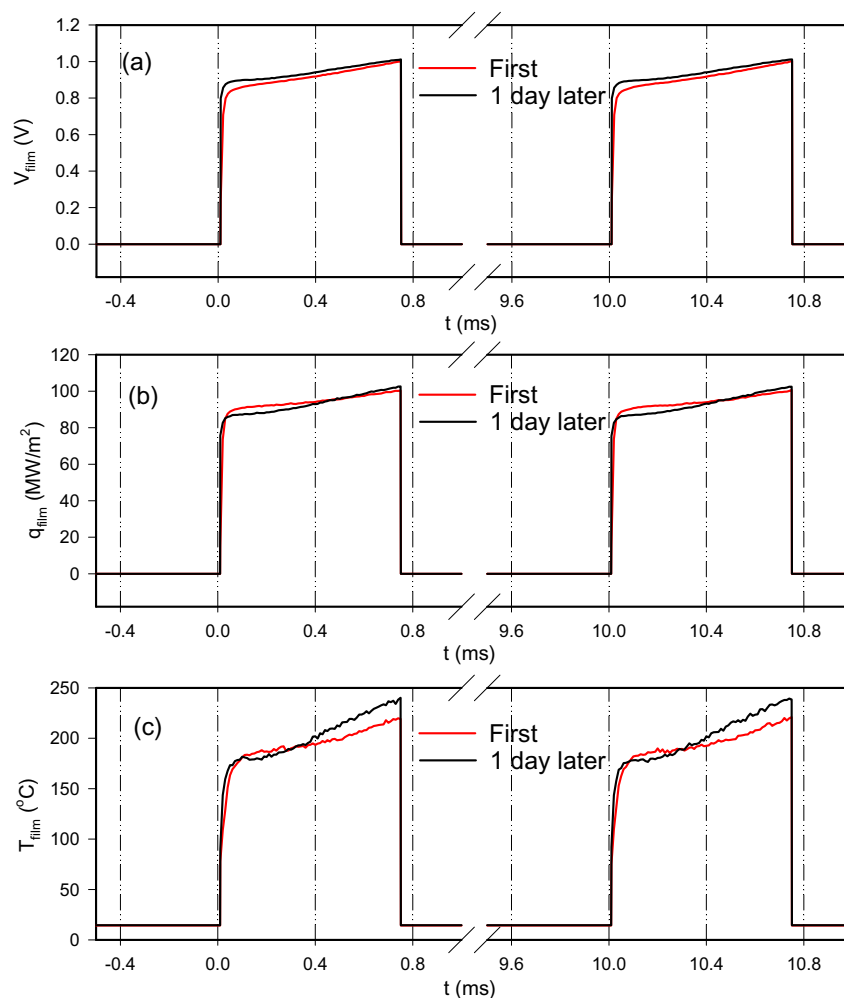


Fig. 13. Voltage, heat flux and temperature on the microheater surface with 1% nanofluid weight concentration ($f = 100$ Hz, $\tau = 0.75$ ms).

several days operation of experiments (see Fig. 1d). Generally, for each given set of pulse heating parameters, the experiments are performed for three times in different days. The experiments are well repeated. Even though the particle coalescence begins to form for the weight concentration of 0.5%, but the particle deposition on the heater surface is not observed. The situation is changed for the weight concentration of 1.0%, in which the particle deposition phe-

nomenon is identified in Fig. 1e. Figs. 13 and 14 show the dynamic curves of voltages, heat fluxes, temperatures and bubble images versus time. Two sets of experimental data are given in Fig. 13. One set of data is obtained for the first day, the other for one day later. The voltage and heat fluxes are almost the same for the two days operation. The temperatures of the microheater are changed. It is seen from Fig. 13 that the temperatures are increased by

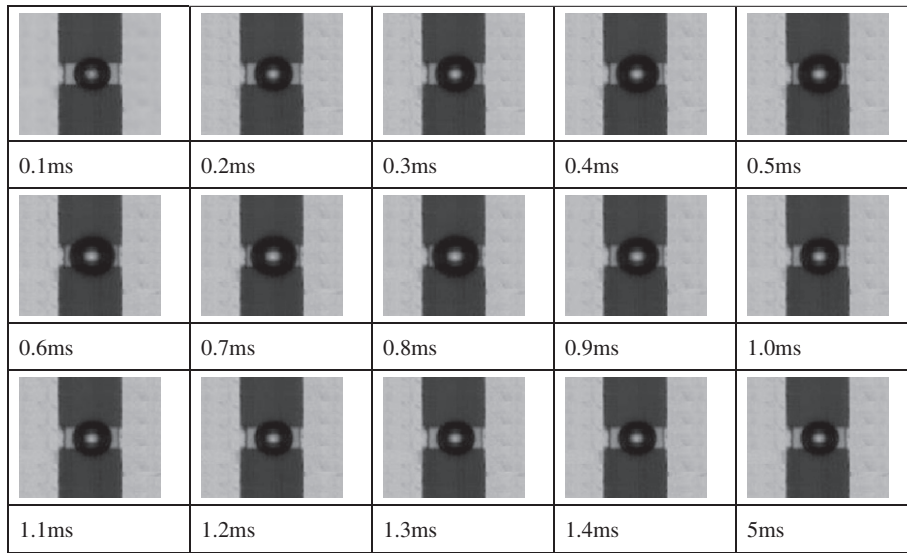


Fig. 14. Bubble images with 1% weight concentration of nanofluid ($f = 100$ Hz, $\tau = 0.75$ ms).

about 20 °C at the end of pulse duration stage for the second day operation. This is due to the increased contact thermal resistance between the heater surface and the nanofluids. There is a thin coated particle layer between the heater surface and the nanofluids. The bubble dynamics shown in Figs. 13 and 14 belong to the third type of bubble dynamics.

Fig. 15 shows the microheater temperatures versus time in pure water ($wt = 0$), and nanofluids with the weight concentrations of 0.1%, 0.2%, and 0.5%, respectively. The heat fluxes are in the range of 86–117 MW/m² in each subfigures. The temperature curves have similar shape at different heat fluxes for a specific weight concentration of nanofluids. Fig. 15a belongs to the first type of bubble dynamics in pure water, in which the temperatures are increased with increases in the heat fluxes. Fig. 15b and c illustrate the second type of bubble dynamics for the nanofluid weight concentration of 0.1% and 0.2%. The higher the heat fluxes, the larger the microheater temperatures are. But the microheater temperature curves are overlapped for different heat fluxes (see Fig. 15c). Generally the sensitivity of the heat fluxes on the microheater temperatures becomes smaller with nanoparticles than that without nanoparticles. Fig. 15d shows the third type of bubble dynamics for the weight concentration of 0.5%, in which the curve shape is similar to that in pure water. But the temperatures are lower in nanofluids than those in pure water without nanofluids.

4.5. Physical explanation of the pool boiling heat transfer in pure water and nanofluids

4.5.1. Explanation for the bubble size with and without nanoparticles

Fig. 16a shows a bubble on the heating surface without nanoparticles. The force balance under a uniform heat flux boundary condition can be written as [15]

$$p_l - p_v = -\frac{\sigma(d^2h/dx^2)}{[1 + (dh/dx)^2]^{3/2}} + \Delta\rho gh + \frac{q_{\text{film}}^2}{2\rho_v h_{\text{lv}}^2} \quad (7)$$

where p is the pressure, l and v are the liquid and vapor phases, respectively, h is the film thickness, q_{film} is the heat flux. The first term of the right hand side is the capillary contribution to the pressure difference, the second term is the gravitational contribution, and the third term is due to the heating effect. Fig. 16b is a bubble when the nanofluid is involved. In terms of the study by Wasan and Hikalov [15], the forces applied on the interface film near the solid–

liquid–vapor contact line are changed with nanoparticles. A structural disjoining pressure should be considered to modify Eq. (7) [16]:

$$p_l - p_v = -\frac{\sigma(d^2h/dx^2)}{[1 + (dh/dx)^2]^{3/2}} - \Pi(h) + \Delta\rho gh + \frac{q_{\text{film}}^2}{2\rho_v h_{\text{lv}}^2} \quad (8)$$

where $\Pi(h)$ is the structural disjoining pressure. The structural disjoining pressure pushes the solid–liquid–vapor contact line toward the vapor side, decreasing the contact area between the heating surface and the dry vapor.

In terms of the classical bubble dynamics theory, the balance between the buoyancy force, surface tension force and inertia force determines the bubble growth and departure process, in which the buoyancy force causes the bubble departing from the heating surface, the surface tension force and inertia force adhere the bubble on the heating surface. The balance among the three forces are written as

$$\vec{F}_\sigma + \vec{F}_l = \vec{F}_g \quad (9)$$

During the bubble growing process, the buoyancy force is being increased due to the bubble volume increase. At the same time, the contact area between the heating surface and the vapor phase is also increased. From the expression $F_\sigma = \sigma D_B \pi \sin \theta$, the surface tension force is increased. Considering the bubble dynamics with nanoparticles involved (see Fig. 16b), the structural disjoining pressure decreases the diameter D_B of the contact area between the heating surface and the dry vapor, causing the decreased surface tension force. This effect decreases the bubble size before the bubble departs from the heating surface with nanofluids. In other words, the nanofluids cause the easy bubble departure from the heating surface. This is the reason why we always observe miniature bubbles on the microheater and the bubble thoroughly disappears during the pulse off stage. This is true for the pool boiling of nanofluids with the weight concentrations of 0.1% and 0.2% in this study.

Now we give the reason why larger bubble is also observed for the weight concentration of 0.5%. Based on Trokhymchuk et al. [17], the structural disjoining pressure can be written in the following form in terms of the Ornstein–Zernike equation.

$$\Pi(h) = \Pi_0 \cos(\omega h + \phi_2) e^{-\kappa h} + \Pi_1 e^{-\delta(h-d)}, \quad h \geq d \quad (10a)$$

$$\Pi(h) = -P, \quad 0 < h < d \quad (10b)$$

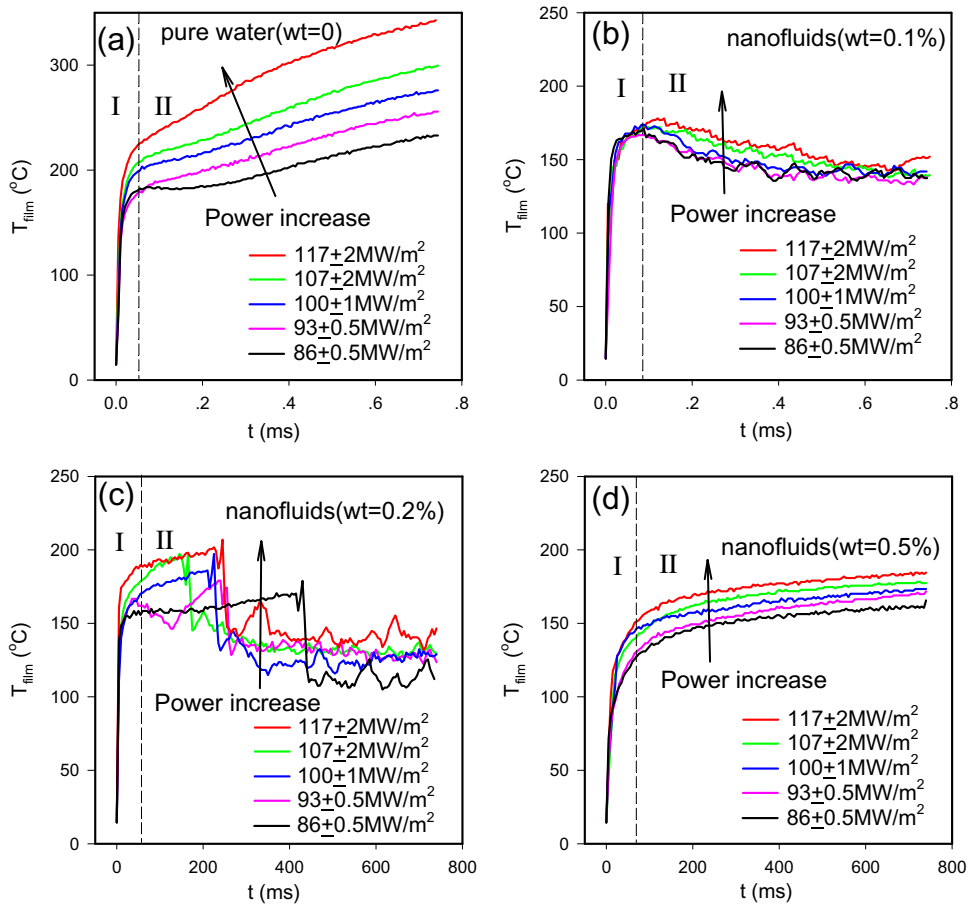


Fig. 15. Effect of heat flux on the microheater temperatures at various weight concentrations.

where h is the thin film thickness near the solid–liquid–vapor contact line, d is the particle diameter. The other parameters in Eq. (10a) are related to the volume fraction of the nanoparticles, and κ , ω , δ , ϕ_2 , Π_0 and Π_1 are the Debye length, frequency of the oscillation, short-range decay parameter, phase of oscillations, amplitude coefficients, respectively. Based on the analysis by Nikolov et al. [18], increasing the nanoparticle concentration, or decreasing the particle size, could increase the structural disjoining pressure, leading to the further decreased contact area between the heating surface and the dry vapor. Fig. 17a shows the decreased D_B by increasing the nanoparticle concentrations, and Fig. 17b shows the decreased D_B by decreasing the particle size. This analysis is in conflict with the observations for the weight concentration of 0.5% in this study. A possible explanation is made here that high

weight concentration of nanofluids such as 0.5% leads to the easy coalescence due to the Brownian movement of particles, ensuring the mixing of several particles to form a large particle. As shown in Fig. 17b, large particle size will enlarge the contact area between the heating surface and the bubble, increasing the surface tension force effect, adhering the bubble on the heating surface. This is the reason why large bubble is observed on the microheater surface even during the pulse off stage for the weight concentration of 0.5%.

4.5.2. Explanation for the heat transfer behavior with and without nanoparticles

It is well known that there are three heat transfer mechanisms for the boiling heat transfer: (1) the thin liquid film evaporation heat transfer; (2) the heat transfer due to the interchange of the

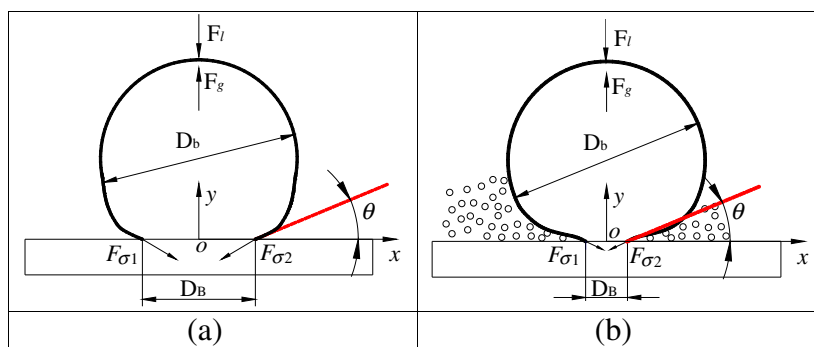


Fig. 16. Force balance acting on the growing bubbles (a) the pure water run and (b) the nanofluid run.

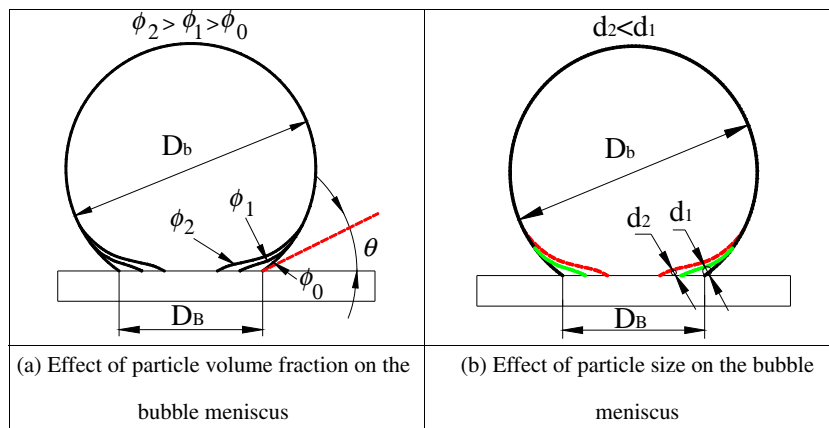


Fig. 17. Effect of particle volume fraction and size on the bubble meniscus.

hot and cold liquids during the bubble departure process; (3) the micro-convection heat transfer due to the disturbance of the boundary layer during the bubble departure process. It is noted that the above three heat transfer mechanisms exist for the boiling heat transfer in pure water. When the low concentration nanofluids (for example, $wt = 0.1\%$ and 0.2%) are involved, the contact area between the heater surface and the dry vapor phase is decreased, causing the smaller bubble size departing from the heater surface. The bubble departure frequency is also increased. These factors cause the enhanced thin liquid film evaporation heat transfer due to the enlarged thin liquid film area, the enhanced heat transfer due to the interchange of the hot and cold liquids during the bubble departure process because miniature bubbles are more frequently released from the heater surface, and the enhanced micro-convection heat transfer due to the enhanced disturbance of the boundary layer during the bubble departure process. Therefore, enhanced boiling heat transfer is identified for the weight concentrations of 0.1% and 0.2% , compared to the pure water runs. This analysis is suitable for the no particle coalescence and deposition on the heater surface.

Even though large bubbles are observed on the microheater surface in both pure water and nanofluids of 0.5% weight concentration, the heat transfer mechanisms are different under the two conditions. Fig. 18 helps to identify the difference between the pure water run and the nanofluids run of 0.5% weight concentration. When a bubble is growing on the heater surface without nanoparticles, there are three heat transfer zones (see Fig. 18a): (1) zone I represents the heater surface directly exposed in the vapor phase (called dry zone); (2) zone II is the thin liquid film evaporation zone; and (3) zone III is the liquid zone with the heater surface exposed in the bulk liquid region. Fig. 18c shows the heat transfer coefficient distribution for the three heat transfer zones, in which zone I has very small heat transfer coefficient due to the heater surface exposed in the vapor phase, while zone II has significant contribution to the overall heat transfer.

On the other hand, when a bubble is growing on the heater surface with nanoparticles involved, Fig. 18a should be modified to form Fig. 18b, showing the heat transfer image. There are four zones in Fig. 18b: (1) zone I is the dry zone; (2) zone II is the thin liquid film evaporation zone in which no nanoparticles are involved; (3) zone III is the zone with the heater surface exposed in the bulk nanofluid region; and (4) zone IV is the thin liquid film evaporation zone in which nanofluids are involved.

The larger heat transfer coefficients for the weight concentration of 0.5% is due to the following reasons: (1) zone I behaves very small heat transfer coefficient and it is significantly shortened for the nanofluid weight concentration of 0.5% ; (2) zone IV, which

has higher heat transfer coefficient, does not exist for pure water run but exists for nanofluids run.

For the weight concentration of 1.0% , particle deposition on the heater surface causes an additional particle layer between the heater surface and the nanofluids, resulting in an increased contact thermal resistance underneath the nanofluids. Thus the boiling heat transfer performance is poorer for the 1.0% weight concentration than that for the 0.5% weight concentration, but it is better than that of pure water.

5. Conclusions

The pool boiling heat transfer on the microheater surface with and without nanoparticles by pulse heating was studied. The nanofluids had the weight concentrations of 0.1% , 0.2% , 0.5% , and 1.0% . The Al_2O_3 particles are mixed with de-ionized water to form the nanofluid. Three types of bubble dynamics were identified:

- For the first type of bubble dynamics for the boiling in pure water, large bubble is observed on the microheater surface and it is still on the microheater surface during the pulse off stage. The microheater temperatures are sharply increased once a new pulse cycle begins, they are increased continuously during the pulse duration stage.
- The second type of bubble dynamics is found for the 0.1% and 0.2% nanofluid weight concentrations. The microheater temperature has a sharp increase at the start of a new pulse cycle, followed by a slight decrease during the pulse duration stage. Miniature bubble has oscillation movement along the microheater length direction, and it disappears during the pulse off stage.
- The third type of bubble dynamics for the 0.5% and 1.0% nanofluid weight concentration behaves the similar bubble behavior for the pure water runs. But the microheater temperatures are lower than that in pure water.
- A structural disjoining pressure causes the smaller contact area between the dry vapor and the heater surface, decreasing the surface tension force effect and resulting in the easy departure of miniature bubbles for the 0.1% and 0.2% nanofluid weight concentrations.
- For the 0.1% and 0.2% nanofluid weight concentrations, the heat transfer mechanisms during the bubble on the heater surface and the bubble departure process are responsible for the higher heat transfer coefficients.
- For the 0.5% nanofluid weight concentration, coalescence of nanoparticles to form larger particles is responsible for the large bubble formation on the heater surface.

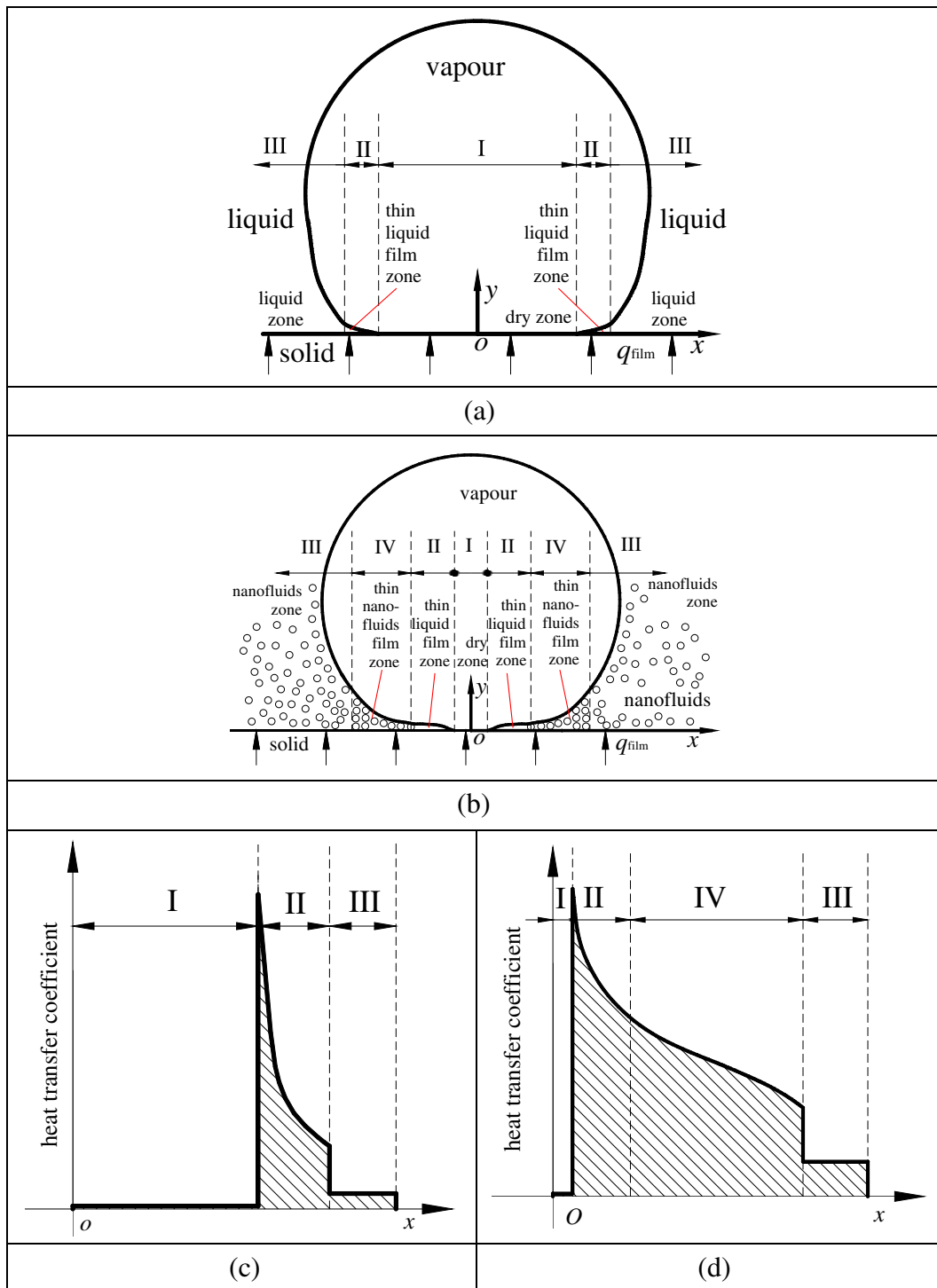


Fig. 18. Heat transfer region and heat transfer coefficient distribution with and without nanoparticles (the figure is re-plotted based on Ref. [15]).

- The shortened dry area between the bubble and the heater surface, and the thin nanofluid liquid film evaporation heat transfer account for the higher heat transfer coefficient for the 0.5% nanofluid weight concentration, compared with the pure water runs.

Acknowledgments

This work is supported by the National Science Fund for distinguished young scholars from National Natural Science Foundation

of China (No. 50825603), National Natural Science Foundation of China (No. U1034004) and the National Basic Research Program of 973 with the contract number of 2011CB710703.

References

- [1] S.U.S. Choi, Enhancing thermal conductivity of fluids with nanoparticles, in: Proceedings of the 1995 ASME International Mechanical Engineering Congress and Exposition, San Francisco, CA, USA, 1995.
- [2] S. Kaka, A. Pramuanjaroenkij, Review of convective heat transfer enhancement with nanofluids, *Int. J. Heat Mass Transfer* 52 (2009) 3187–3196.
- [3] W. Daungthongsuk, S. Wongwises, A critical review of convective heat transfer of nanofluids, *Renew. Sust. Energ. Rev.* 11 (2007) 797–817.

- [4] I.C. Bang, S.H. Chang, Boiling heat transfer performance and phenomena of Al_2O_3 -water nanofluids from a plain surface in a pool, *Int. J. Heat Mass Transfer* 48 (2005) 2407–2419.
- [5] M.N. Golubovic, H.D.M. Hettiarachchi, W.M. Worek, W.J. Minkowycz, Nanofluids and critical heat flux, experimental and analytical study, *Appl. Therm. Eng.* 29 (2009) 1281–1288.
- [6] S.J. Kim, T. McKrell, J. Buongiorno, L.W. Hu, Experimental study of flow critical heat flux in alumina-water, zinc-oxide-water, and diamond-water nanofluids, *J. Heat Transfer* 131 (2009), 043204-1.
- [7] S.J. Kim, T. McKrell, J. Buongiorno, L.W. Hu, Subcooled flow boiling heat transfer of dilute alumina, zinc oxide, and diamond nanofluids at atmospheric pressure, *Nucl. Eng. Des.* 240 (2010) 1186–1194.
- [8] T.N. Dinh, J.P. Tu, T.G. Theofanous, Burnout in high heat flux boiling: the hydrodynamic and physical-chemical factors, 42nd AIAA Aerospace Sciences Meeting and Exhibit, 5–8 January 2004, Reno, Nevada.
- [9] D.S. Wen, Y.L. Ding, Experimental investigation into the pool boiling heat transfer of aqueous based γ -alumina nanofluids, *J. Nanopart. Res.* 7 (2005) 265–274.
- [10] D.S. Wen, Y.L. Ding, R.A. Williams, Pool boiling heat transfer of aqueous TiO_2 -based nanofluids, *J. Enhanc. Heat Transfer* 13 (3) (2006) 231–244.
- [11] Z.H. Liu, J.G. Xiong, R. Bao, Boiling heat transfer characteristics of nanofluids in a flat heat pipe evaporator with microgrooved heating surface, *Int. J. Multiphase Flow* 33 (2007) 1284–1295.
- [12] M.A. Kedzierskia, M. Gong, Effect of CuO nanolubricant on R134a pool boiling heat transfer, *Int. J. Refrig.* 32 (5) (2009) 791–799.
- [13] P.G. Deng, Y.K. Lee, P. Cheng, Measurement of micro-bubble nucleate temperature in DNA solutions, *J. Micromech. Microeng.* 15 (2005) 564–574.
- [14] J.L. Xu, W. Zhang, Effect of pulse heating parameters on the microscale bubble dynamics at a microheater surface, *Int. J. Heat Mass Transfer* 51 (2008) 389–396.
- [15] D.T. Wasan, A.D. Nikolov, Spreading of nanofluids on solids, *Nature* 423 (2001) 156–159.
- [16] D.S. Wen, Mechanisms of thermal nanofluids on enhanced critical heat flux (CHF), *Int. J. Heat Mass Transfer* 51 (2008) 4958–4965.
- [17] A. Trokhymchuk, D. Henderson, A. Nikolov, D.T. Wasan, A simple calculation of structural and depletion forces for fluids/suspensions confined in a film, *Langmuir* 17 (2001) 4940–4947.
- [18] C.A. Nikolov, W.D. Trokhymchuk, et al., Spreading of nanofluids driven by the structural disjoining pressure gradient, *J. Colloid Interf. Sci.* 280 (2004) 192–201.